Resolving the thickness of peat deposits with contact-less electromagnetic methods: A case study in the Venice coastland

https://doi.org/10.1016/j.scitotenv.2020.139361

Formatted: Normal, Line spacing: single

# Resolving the thickness of peat deposits with contact-less electromagnetic methods: a case study in the Venice coastland

Boaga J. [(1)], Viezzoli A. [(2)], Cassiani G. [(1)], Deidda G.P. [(3)], Tosi L. [(4)], Silvestri S. [(5)*]

[(1)] Dept. of Geosciences, University of Padova, Padova, Italy
[(2)] Aarhus Geophysics ApS, Aarhus, Denmark
[(3)] Dept. of Civil and Environmental Engineering and Architecture, University of Cagliari, Cagliari, Italy
[(4)] Institute of Geosciences and Earth Resources, National Research Council, Via G. Gradenigo, 6 - 35131 Padova, Italy, luigi.tosi@igg.cnr.it
[(5)] Dept. of Biological, Geological and Environmental Sciences, University of Bologna, Ravenna, Italy
* corresponding author

## Abstract

Peat soils are typical deposits characterizing wetlands and reclaimed farmlands. They are important carbon reservoirs and when degraded (e.g., erosive processes, fires, draining and plowing) massive carbon dioxide volumes are released. This leads to increase greenhouse effect and induce serious land subsidence. Thus, mapping the volume of peat deposits is crucial in order to estimate the carbon mass and the potential release of carbon dioxide and consequent loss in soil elevation. Despite the importance of such estimations, forecasting and quantifying the peat thickness is still a challenge.

Direct sediment coring provides local information that are difficult to extend to large territories. Indirect geophysical methods are unable to resolve lithological contrasts in the presence of saltwater contamination in coastal areas. ~~Indirect geophysical methods are often vanished by the presence of saltwater contamination in coastal areas~~. In this work, we show the results obtained using two contact-less electromagnetic methods for the characterization of peat deposits in a peatland site of the Venice coastland, Italy. Specifically, a multi-frequency portable instrument (FDEM) and an airborne time-domain electromagnetic one (AEM) were used to collect data over a former wetland then reclaimed for agricultural purposes. Additional electrical resistivity tomography (ERT) data, ~~which are~~ known for their very high and relatively low vertical resolution respectively, are used together with sediment core data to assess the effectiveness and accuracy of the contact-less methods. Results show that both FDEM and AEM are very effective in detecting the presence of the peat layer, despite its low thickness (< 2 m) and the high electro-conductive subsoil because of saltwater contamination. However, the AEM method overestimated the peat thickness while the FDEM could accurately resolve the peat thickness even where the layer was thinner than 1 m. When compared to the electrical features extracted from the ERT, discrepancies are on average lower than 30-%; when compared to the borehole data, discrepancies are on average slightly higher than 6-%.

**Commented [DSSP1]:** Line 25: Suggest rephrasing the sentence beginning in this line. The verb "vanish" is poor English usage in this context. Try either of these sentences: "Indirect geophysical methods do not work well in the presence of saltwater contamination in coastal areas." OR "Indirect geophysical methods are unable to resolve lithological contrasts in the presence of saltwater contamination in coastal areas."

## 1. Introduction

Peatlands are important carbon pools and, if degraded, they release large amounts of carbon dioxide and other greenhouse gasses (Page et al., 2002; Turetsky et al., 2015). The organic carbon stored belowground is preserved by wet or moist soil conditions.

Once the soil is drained, as for example during prolonged droughts or for man-induced processes such as land reclamation, aerobic microorganisms decompose quickly the organic matter, releasing carbon dioxide and other gasses (e.g., Hooijer et al., 2012; Fenner and Freeman, 2011). The decomposition of organic matter also induces one of the most severe mechanisms of land subsidence, i.e. the geochemical subsidence (Zanello et al., 2011), which may cause meters of loss in ground elevation in a few decades.

At the global scale, the large majority of terrestrial carbon is stored in soils. It is estimated that vegetation stores about 500 Pg of carbon (considering both aboveground and belowground phytomass) while soils store between 1500 Pg (Scherlemann et al., 2014) and 2500 Pg (Batjes, 2014; Jansson et al., 2010) of carbon, and ~ 30% of it is stored in peatlands (Scherlemann et al., 2014; Bourgeau-Chavez et al., 2018). Peat degradation has been proven to contribute an enormous amount of greenhouse gasses to the atmosphere every year. The estimate of the global emission of $CO_{2eq}$ due to peatland drainage is very uncertain, and varies between 0.9 and 1.3 Gt $CO_{2eq}$/yr (Joosten, 2010; FAOSTAT, 2013). This picture is even more alarming if we consider that the numerous fires that occur in forested wetland systems, especially in tropical areas, increase the amount of greenhouse gasses released every year (Turetsky et al., 2015; Ballhorn et al., 2009). In addition to the problems related to $CO_{2eq}$ emissions, the continuous conversion of tropical peatlands to agriculture and the hydraulic drainage of low-lying areas have resulted in widespread land subsidence creating great concern especially in coastal areas (e.g., Van Asselen et al., 2018).

Considering that the potential of releasing carbon dioxide and of peatland subsidence depends on the mass availability of the organic matter in the soil, the quantification of the peat extent over vast territories is a very relevant challenge. Therefore, it is

becoming urgent to develop methodologies that allow an accurate and fast mapping of soil organic carbon, with particular interest for wetlands and peatlands.

The most common and widely used method for peat deposit quantification and characterization relies on shallow borehole information and ground-based surveys using geophysical methods. In order to be effective at the regional scale and given the extent and thickness variability of peat, a method based on field measurements needs a large database of high-density distributed field observations, which are essential in order to correctly define the covariance model necessary to interpolate/extrapolate the point measurements (Keaney et al., 2013) and minimize spatial aliasing. In the literature, there are examples of studies reporting the collection of a large number of peat thickness measurements performed in the field using push probes (Parsekian et al., 2012; Householder et al., 2012; Holden and Connolly, 2011). However, even though the use of push probes is a relatively fast method and may provide large databases, it has been shown that the accuracy reached using exclusively soil probes is limited, leading to an average error of depth estimation as high as 35% (Parry et al., 2014). Soil coring guarantees much higher accuracies in measuring the peat thickness locally, however it is extremely time consuming especially in wetland environments and does not allow the collection of large enough databases. In order to overcome these issues, various traditional ground-based geophysical techniques have been successfully applied for peat characterization. For example, ground penetrating radar (GPR) (e.g., Comas et al. 2017; Comas et al., 2015; Parsekian et al., 2012; Slater and Reeve, 2002), electrical tomography (ERT) (e.g., Walter et al. 2019; Comas et al., 2015; Elijah et al., 2012; Boon et al., 2008;) and induced polarization (IP) methods (e.g., Comas and Slater, 2004; Slater and Reeve, 2002) together with complementary borehole data.

**Commented [DSSP2]:** Line 95: change complement to complementary

Nevertheless, the use of soil cores and traditional ground-based geophysical techniques are generally limited, being moist and wet soil conditions difficult accessible and the relatively local scale of the investigations obtainable. Moreover, the presence of dense vegetation cover ~~peatlands are usually covered with very dense vegetation that~~ represents an additional challenge for traditional ground-based geophysics.

Recently, Silvestri et al. (2019a, 2019b) used airborne electro-magnetic (AEM) to identify peat layers over large territories in a Norwegian study site characterized by the presence of several bogs and in a large Indonesian peatland respectively. In both these frameworks, the AEM method proved to be highly effective to distinguish the electrical properties of the peat layer from that of the substrate, allowing delineation of their boundaries~~allowing to drawn their boundary~~. Higher vertical resolution is obtained with the presence of conductive substrate while the uncertainty increases for resistive substrates. However, through a sensitivity analysis, Silvestri et al. (2019a, 2019b) show that the accuracy reached using exclusively the AEM method is generally not sufficient to resolve thin peat layers, roughly 1-1.5 m thick. Therefore, an alternative approach is needed to investigate thin peat layers over large areas.

In this paper, we present the results obtained by testing for the first time a contact-less frequency domain electromagnetic method (FDEM) for resolving the peat thickness. The main advantage of this method is that it is suitable for meso-scale peatland characterization of difficult-to-access areas, but also tries to overcome the limited vertical resolution that affects the AEM technology. A comparison of the vertical accuracies obtained with both AEM and FDEM methods is also performed and discussed~~.~~

The pilot area selected for this study is a low-lying peatland used for farmland, located between the Po river delta and the Venice Lagoon, Italy. Most of the farmland is derived

**Commented [DSSP3]:** Lines 98-99. Check English in the second phrase of this sentence

**Commented [DSSP4]:** Lines 106-107. Change the phrase "allowing to drawn their boundary" to "allowing delineation of their boundaries."

from the hydraulic reclamations of ancient wetlands and lagoons, which started at the beginning of the last century, and today lies below mean sea level.

Information on the peat thickness is very limited as it is available only from sediment cores, which provide local details. In general, the peat layer thickness is lower than 2 m because the original uppermost layers were oxidized during the last century due to the hydraulic drainage and agricultural activities, which induced geochemical subsidence (Tosi et al., 2009). Tosi et al. (2000) computed rates of up to 3-4 cm/yr of loss in elevation during the last century. Such large historical rates come from a number of concomitant causes of land subsidence that included (i) the groundwater pumping occurred in the 1950-1960 period (contributing about 1-1.5 m to the total subsidence), (ii) exploitation of gas-bearing waters (from late 1940s to late 1960s), (iii) the common practice of burning grass and vegetation that grew along the banks of the hydraulic drainage network causing the peat to burn. In addition, the maintenance of a very low water table (by pumping stations) during rainy periods in order to avoid sudden floods increased for decades the oxidation of organic soils and therefore facilitated the geochemical subsidence. Today, groundwater exploitation and the agriculture practice of burning vegetation are no longer used, and the beginning of 2000's the hydraulic reclamation drainage management allows to keep the water table higher than in the past, significantly reducing land subsidence rates. Even though the rates are considerably smaller than in the past, it has been shown that the land is still subsiding at a rate of 3-15 mm/yr, calculated for the recent years (Zanello et al., 2011) releasing in the atmosphere 9.2 ± 5.5 kg $CO_2$ $m^{-2}$ $yr^{-2}$ (Camporese et al., 2008).

The selected case study is particularly challenging from the geophysical point of view because thin peat deposits are hard to distinguish from the underlying conductive substrate that consists of clay and silty-clay layers, often salinized by saltwater

intrusion. In fact, the organic matter present in peat soils has similar electrical properties to conductive substrates (Silvestri et al. 2019b), producing a modest resistivity contrast that makes it problematic to detect the discontinuity at the bottom of the peat. Despite the challenges, our findings show that contact-less geophysical methods as FDEM and AEM can successfully detect the presence of peat deposits. While AEM tends to overestimate the peat thickness of thin peat deposits, FDEM can accurately resolve also very thin peat layers.

## 2. Study site

The study site is the Zennare basin, which is part of a larger low-lying area located between the southern margin of the Venice Lagoon and the northern Po river delta (Italy) (Fig. 1). The area is characterized by Holocene deposits with a variety of geomorphic features, as for example ancient fluvial ridges, paleo-river beds and paleo-coastlines (Rizzetto et al. 2003). The basin is currently below the mean sea level and it mostly consists of high value agricultural land established after the hydraulic reclamation of pre-existing lagoons and wetland areas that started in the Veneto Region in 1892. Today, the basin is surrounded by levees; ditches regulate the surface waters and pumping stations stabilize the water table at about 0.5 m below the land surface, discharging the drainage water into the Venice Lagoon or the Adriatic Sea.

Over the past century, oxidation of the organic soil fraction in response to drainage for farming provoked the degradation of the shallow peat deposits leading to serious land subsidence rates, often one order of magnitude higher than the natural ones caused by sediment compaction and tectonic movements (e.g., Tosi et al., 2009; Tosi et al., 2010; Tosi et al., 2016). Evidence of peat-oxidation land settlements, e.g., the protrusion of

old hydraulic structures founded on the stiff clays and sands underlying the outcropping peat, and ground- and satellites-based monitoring data allowed to quantify up to 2-3 cm/yr of loss in surface elevation (Tosi et al., 2000; Gambolati et al., 2005; Tosi et al., 2016). Consequently, the basin today lays between 2 and 4 m below the mean sea level (Rizzetto et al., 2003; Gasparetto-Stori et al., 2012). Ridges corresponding to sand filled paleochannel systems not affected by geochemical subsidence due to oxidation of the organic matter show higher elevations than the nearby peat soils.

The outcropping peat deposits extend for most of the basin (e.g., Nicoletti et al., 2003). The large majority of the shallow peats originally present in the area have been degraded due to geochemical subsidence as consequence of the oxidation of the organic soil. Currently the thickness of the peat layer is almost half of the original one and varies between less than 1 m to a maximum of 2 m across the basin (Rizzetto et al., 2003).

The shallow sequence is constituted by a c.a. 50 cm of ploughed and oxidized soil at the top and a peat with well-preserved fibers in growing position at the bottom. At the base, there is a transition layer of clayey peat gradually passing to clay with spread vegetable remains (Gatti et al., 2001). Peats derive from the accumulation of reeds (Phragmites australis) living in wetlands before the reclamation (Gatti et al., 2001).

Soil salt contamination partly affects the Zennare Basin (e.g., Rizzetto et al., 2003). The saltwater intrusion is favored by the land elevation that is well below the mean sea level but also by the presence of sandy paleo-channels crossing the farmland with main direction from inland to the lagoon boundary.

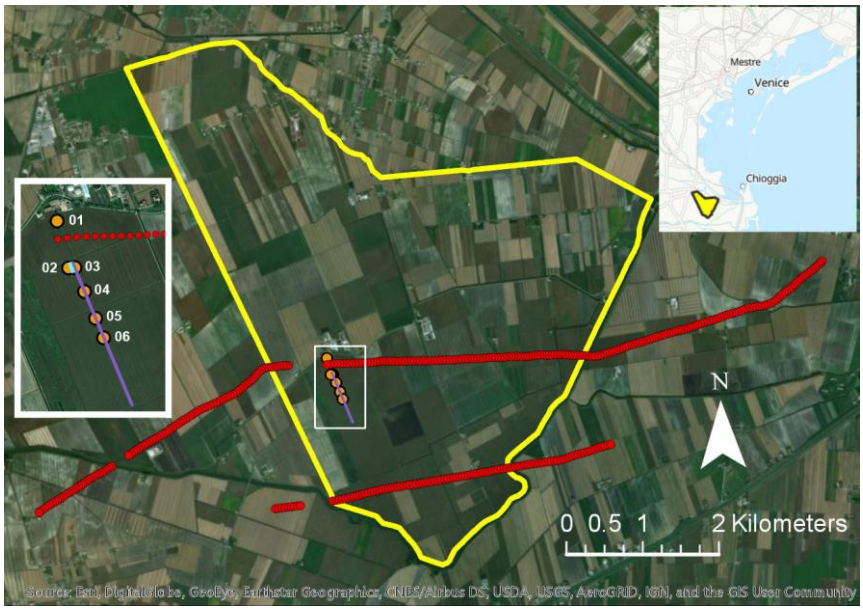


Fig. 1 – The Zennare basin is outlined in yellow. The map inset on the top-right shows the location of the basin with respect to the Venice lagoon (Italy). The red lines correspond to the AEM flight lines. The white rectangle shows the location of the ground-based field surveys and is magnified within the inset to the left of the figure, where the orange dots indicate the shallow boreholes, the purple line corresponds to the FDEM transect and the short light-blue line shows the location of the ERT transect.

## 3. Methods

The dataset collected and analyzed in this study includes (see Fig. 1 for locations): (i) frequency domain ground-based electro-magnetic (FDEM) data, (ii) ERT data along the initial portion of the FDEM transect, (iii) an aerial AEM survey along 2 flight-lines, and (iv) borehole data collected along the FDEM transect, in order to get lithological information and peat layer thickness.

With reference to other studies carried out in the Venice coastland (e.g., Carbognin et al., 2003; de Franco et al., 2009; Viezzoli et al., 2009; Teatini et al., 2011; Da Lio et al., 2015), electrical resistivity <5 Ω·m and >10 Ω·m are respectively the upper and lower values for saltwater and freshwater, in terms of the electro-lithological units.

### 3.1 Frequency Domain Electro-Magnetic (FDEM) survey

The FDEM survey was performed in Fall 2018 using a GEM-2 probe manufactured by Geophex (www.geophex.com). The FDEM system is a multi-frequency probe, capable of investigating electrical properties of several depths at the same time (e.g., Boaga, 2017, 2018; Deidda et al., 2014). The probe has one transmitter and one receiver coils, with a fixed separation of 1.66 m, and a multifrequency operation in the bandwidth 30 Hz - 93 kHz. GEM-2 can be used as a conductivity meter for depth sounding when it operates in a range of moderate induction number (McNeill, 1980), for which the responses are strong and frequency dependent (Huang and Won, 2003). To meet this requirement, as the area is underlined by fairly conductive sediments, we used six frequencies ($f_1$= 1,250 Hz, $f_2$ = 4,250 Hz, $f_3$ = 10,025 Hz, $f_4$ = 21,750 Hz, $f_5$= 30,025 Hz, and $f_6$ = 47,025 Hz) in order to span the range of induction numbers between 0.1166 and 0.7152, and assuming the worst condition of a nonmagnetic half-space with a conductivity equal to 1 S/m.

The GEM-2 probe was carried by the operator along a 700 m NW-SE transect (see Fig. 1 for location), at a constant height of about 1 m from the surface. The FDEM probe was connected to a Trimble GPS receiver to record the spatial coordinates for each measurement (with a total of about 12,000 points). Raw data were then processed focusing on the area where ERT data and control boreholes (03 and 04) are available (see section 3.3).

Prior to the inversion, data collected along the first 200 m of the transect were spatially resampled at 1 m interval to set up a data set consisting of a series of 201 geometric depth soundings with six complex (quadrature and in-phase components) GEM-2 responses. The complex response recorded at each sounding point was individually inverted to infer the electrical conductivity depth profile using the FDEMtools (Deidda et al., 2019), a free MATLAB software package implementing the numerical algorithms mainly discussed by Deidda et al. (2014, 2017).

A layered starting model, with the layer conductivities based on ERT results, was used for all one-dimensional inversions. In addition, to best fit the in-phase data at lower frequencies, the relative magnetic permeability was set at 0.995 (i.e., a magnetic susceptibility of – 0.005, a value representative of diamagnetic materials) in the top 1 m portion of the model. As shown in Deidda et al. (2020), in this case too the inversion of the complex signals has provided better results than the inversion of the quadrature (imaginary part) component of the secondary to primary magnetic field ratio alone, reaching root mean squared errors lower than 10%. Fig. 2 shows two examples of data fitting, which relate to electromagnetic soundings co-located with boreholes 03 (Fig. 2a) and 04 (Fig. 2b).

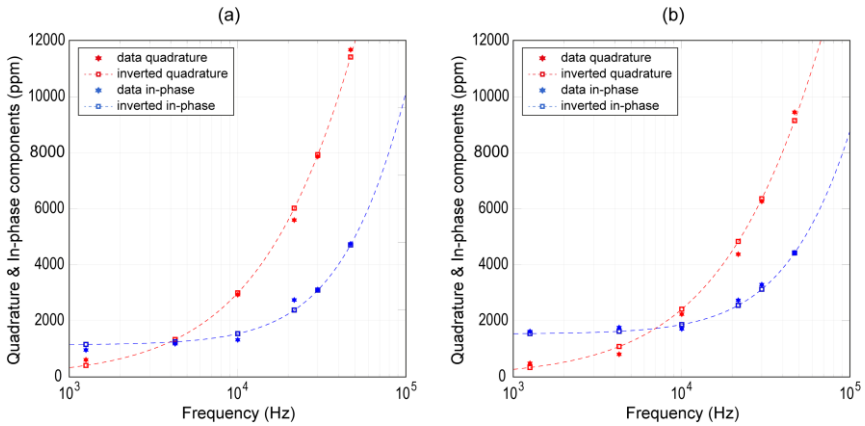

Fig. 2 – Quadrature (red) and in-phase (blue) components of the secondary magnetic field response (ppm of the primary) as a function of frequency for electromagnetic soundings at 24 m (a) and 142 m (b) from the beginning of the FDEM transect. Stars and squares represent measured and predicted data, respectively.

### 3.2 Electrical Resistivity Tomography (ERT) data

Along the first portion of the selected transect we also acquired an ERT transect with the purpose of calibrating and comparing the resulting electrical resistivity values with those obtained using the FDEM method. We adopted a 48 electrodes setup with 0.5 m electrode spacing, for a total ERT length of 23.5 m. This ensures a depth of investigation of about 5 m (1/4-1/5 of the ERT line length).

We used a dipole-dipole skip 0 configuration – i.e. with dipole lengths equal to the minimum electrode spacing - collecting both direct and reciprocal measurements, in order to control the quality of the raw data (e.g., Cassiani et al., 2006). Data were collected with a Iris Instrument Syscal Pro resistivity meter, and were then inverted using the R2 code (e.g., Binley, 2015). The collected dataset is of high quality, since the 96% of the data pass the reciprocals check using a 5% error threshold.

### 3.3 Airborne Time Electro-Magnetic (AEM) data

Airborne Time Electro-Magnetic (AEM) data were collected in Fall 2013 in the context of the National Flagship Project RITMARE (Tosi et al., 2018). The project aimed at providing a step forward in the delineation of the continental and marine surface water–groundwater interactions and the mechanisms controlling the saltwater intrusion, overcoming the intrinsic constrains typical of ground-based surveys. Within the

RITMARE framework, the SkyTEM helicopter-deployed time domain electro-magnetic system was chosen as its dual moment provides a bandwidth (i.e. a penetration range) suitable for applications where both near-surface and deep information is important to refine the hydrogeologic model (e.g., Teatini et al., 2011; Sørensen & Auken, 2004). During the flight, current flows through a transmitter loop carried below the helicopter at an altitude of about 30 m, setting up a magnetic field. The eddy currents induced below the ground surface generate a secondary magnetic field, and a receiver coils on the frame detects its temporal variation. SkyTEM data have been recently proven very effective in characterizing peatlands in boreal and tropical areas (Silvestri et al. 2019a, 2019b).

The AEM data have been re-processed in order to attempt to maximize the accuracy for the detection of the near-surface soil layers. The data have then been inverted using two homogeneous starting models, with initial conductivity of 30 Ω·m and 5 Ω·m. For both cases, the inversion was performed using 40 and 5 layers.

### 3.4 Shallow borehole data

The field surveys were performed in Fall 2018 and Spring 2019. The thickness of the peat layer was measured at six locations localized using GPS (Tab. 1). The samples were retrieved using an auger peat corer with diameter of 2.5 cm and 50 cm length. Mechanical extensions were used in order to reach the bottom of the peat layer and characterize the transition surface towards the sand below. A small sample of substrate was collected at each location in order to determine its characteristics.

Geological and hydrogeological data collected within previous research projects and available through the websites of Città Metropolitana Venezia

(http://webgis.cittametropolitana.ve.it/geologia) have also been used to support the validation and interpretation of the geophysical outcomes.

## 4. Results

Tab. 1 summarizes the outcomes for all the boreholes and includes a sample lithology corresponding to borehole 01 (see Fig. 1 for location). All shallow boreholes show a similar lithology, which includes a layer of peat in the uppermost portion, with a transition zone characterized by mud mixed with peat and silty-clay underneath.

The thickness of the peat deposits is very thin and has a pronounced spatial variability ranging from 83 cm (borehole 06) to 210 cm (borehole 2) (Tab. 1), with an average value of 134 cm and standard deviation of 54 cm.

The analysis of other cores taken in the Zennare Basin (Gatti et al., 2001; Carbognin and Tosi, 2003; Città Metropolitana di Venezia) confirms the fairly homogenous lithology with variable thickness of the peat layer. Sands and silts are found only in correspondence of paleo-channels.

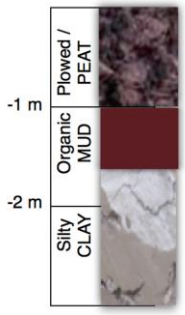


| Borehole ID | Easting coordinate | Northing coordinate | Peat thickness (cm) | Substrate |
|---|---|---|---|---|
| 01 | 12.14083 | 45.17278 | 190 | loamy-clay |
| 02 | 12.14139 | 45.17084 | 210 | silty-clay |
| 03 | 12.14176 | 45.17084 | 130 | silty-clay with fine sand |
| 04 | 12.14226 | 45.16984 | 95 | silty-clay |
| 05 | 12.14283 | 45.16873 | 98 | silty-clay |
| 06 | 12.14325 | 45.16791 | 83 | silty-clay |

Tab. 1 – Data corresponding to the boreholes and sample lithology found for borehole 01.

As explained in the Methods section, we inverted the multi-frequency FDEM data collected along a 200 m long transect overlapping the ERT line and the control borehole 03 and 04.

The resulting one-dimensional models, with 60 layers to a depth of 6 m below the ground surface, are stitched together and plotted as a pseudo two-dimensional section in Fig. 3. The electrical resistivities vary gradually in the lateral direction, although they have been obtained by inverting data, sounding by sounding, without any lateral constraint. This is in agreement with the ERT evidence shown below in Fig.4. Moreover, in agreement with the borehole information, the FDEM data substantially divide the Zennare subsoil in 2 layers: an upper resistive layer with about 1 m thickness lying on an electrically conductive subsurface. The first, with resistivities up to 50 Ω·m, represents the peat deposits, while the latter, with resistivities less than 12 Ω·m, is representative of the silty/clayey – clayey saturated layers (similar values can be found e.g. in the fine sediments of the Venice lagoon - e.g. Boaga et al., 2014). In this very conductive environment, the peat deposits appear to be more resistive (>12 Ω·m) in agreement with what already observed at other sites (Silvestri et al., 2019a, 2019b; Kowalczyk et al., 2017; Boon et al., 2008). These results confirm a substantial agreement with the information coming from the shallow boreholes, confirming that the average thickness of the peat layer in the study site is ~1.3 m. Specifically, considering the 12 Ω·m resistivity threshold as the bottom of the peat layer and averaging all the thickness values corresponding to such threshold along the transect, we obtain a mean peat thickness of 128 cm, with a difference of 6 cm with the average value calculated from boreholes in that zone.

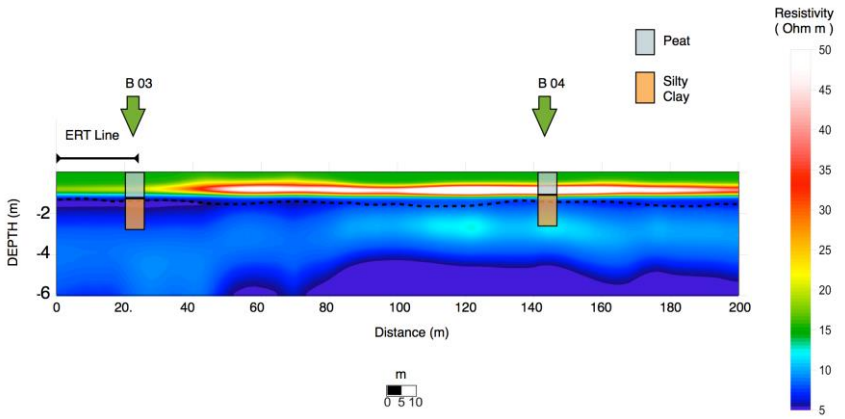


339

340 Fig. 3 - Inverted electrical resistivity profile obtained from the FDEM multi-frequency

341 data. The dashed line indicates the 12 Ω·m contour line as in Fig. 4. The location of the

342 ERT line (Fig. 4) is marked to the left. Tab.1 borehole lithology is also presented.

343

344

345

346

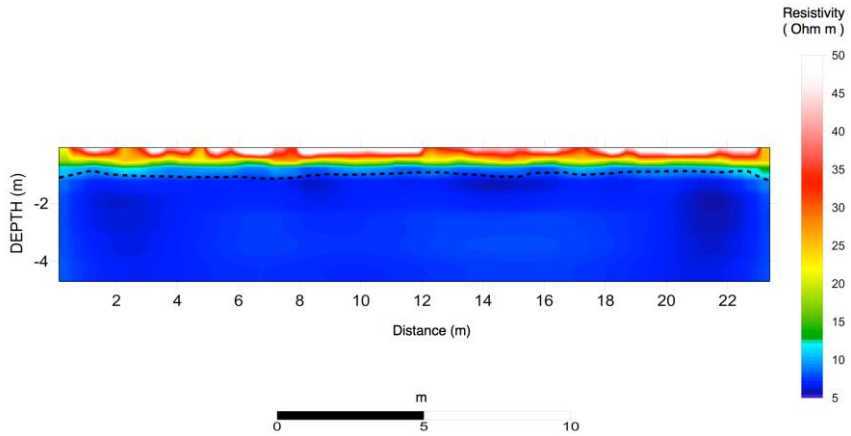


347

Fig. 4 - ERT inverted resistivity section (Fig.1 for location). The uppermost peat layer is more resistive than the underlying silty clay layer having a lower electrical resistivity (< 12 Ω·m). The dashed line indicates the 12 Ω·m contour line as in Fig. 3.

The resistivity values retrieved using the ERT profile are shown in Fig. 4 for comparison with the FDEM inversion in Fig. 3. The ERT and FDEM results agree to a very large extent: the shallow electrically resistive layer (values > 12 Ω·m) lies on a conductive layer below. The contact between the two layers is at about 1 m depth, and this coincides with the transition between the peat and the underlying silty/clay layer (dashed line in Figs. 3-4), as detected by the direct borehole investigations. The ERT data confirm the continuity of the peat layer across the study site with no substantial lateral variations.

The results obtained from the inversion of the longest (northern) AEM flight line (see location in Fig. 1) are shown in Fig. 5. In this case 40 layers and initial conductivity of 30 Ω·m were used. Similar profiles were extracted for the second AEM flight line (the southern one) given the same initial conditions. Other inversions were performed in order to test the consistency of the method, and the results are shown in fig. A1 of the Appendix (i.e. four inversion setups are shown: a) 40 layers and starting with initial conductivity of 30 Ω·m; b) 40 layers and starting with initial conductivity of 5 Ω·m; c) 5 layers and starting with initial conductivity of 30 Ω·m; d) 5 layers and starting with initial conductivity of 5 Ω·m). Note that the initial resistivity value in the inversion has small to no influence on the final resistivity model, indicating that the model quickly loses memory of the initial conditions, and that the inversion is robust. The similarity of the results obtained with the inversions performed using 40 layers and 5 layers tells us that the inversion consistently detects a more resistive surface layer over a

conductive substrate. This indicates that, despite the different resolution capabilities due to the remote sensing setup, the results obtained using the AEM method confirm the presence of an upper resistive layer corresponding to the peat deposit (Fig. 5).

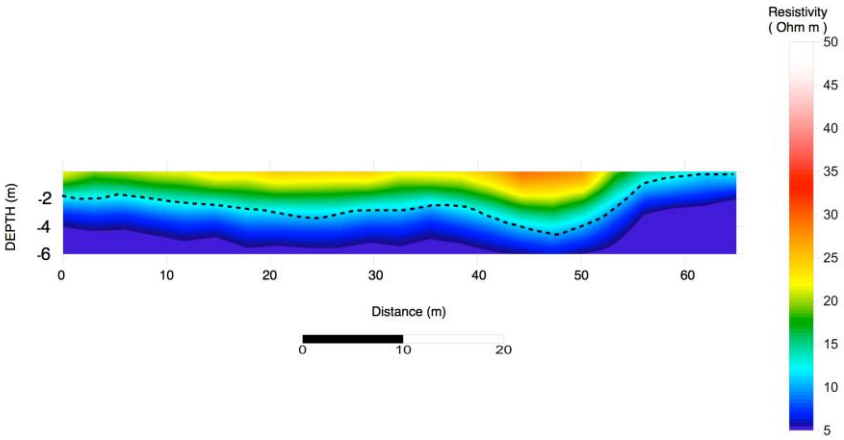


Fig. 5 – Extracted of the AEM results along line A falling within the white rectangle in Fig. 1. Here, like for ERT and FDEM results, the uppermost resistive layer (>12 Ω·m - peat) overlies the more conductive substrate (< 12 Ω·m – silty clay). The dashed line indicates the 12 Ω·m contour line.

Even though the AEM flight-line does not overlap with the ERT and FDEM transects and with the borehole investigations, we can conclude that AEM is in substantial agreement with the results obtained with the other methods. In fact, the AEM method can detect the presence of the peat layer, even though it is very thin, and the resistivity values detected by AEM are in good agreement with those obtained with ground based FDEM and ERT. As for the peat thickness, if we consider the 12 Ω·m resistivity threshold as we did for the FDEM inverted data, we obtain for the AEM data an average peat thickness of 260 cm, which is considerably higher than the average value calculated for FDEM (128 cm) and from boreholes (134 cm). We can conclude that

391 AEM tends to overestimate the peat thickness and this is probably due to a low vertical
392 resolution in a very-near-surface framework.

393

394 **5. Discussion**

395 Coastal wetlands are among the ecosystems that have mostly changed over the last
396 century, especially those converted to agricultural lands by hydraulic reclamations. The
397 soil rich in organic matter and peat layers makes farmlands highly productive, as in the
398 case of the selected study site. However, the drainage systems necessary for keeping
399 the water table level below the ground surface together with the plowing activities, are
400 responsible of massive carbon dioxide release. This process likely increases greenhouse
401 gasses and relative sea level rise because of the geochemical land subsidence triggered
402 by the oxidation of organic matter.
403 Understanding how peatlands contribute to these processes requires detailed knowledge
404 on the peat layer thickness. In general, the areal extent of the peatlands can be retrieved
405 by satellite images (e.g., Nicoletti et al., 2003; Ballhorn et al., 2011; Draper et al., 2014;
406 Jaenicke et al., 2008) while the assessment of their thickness over large areas is a
407 challenge, especially where the peat layer is thinner than 1-2 m and saltwater
408 contamination affect the shallow subsoil. In these environmental conditions, in fact,
409 organic soil, peat and saturated clay are expected to have similar electrical properties.
410 Peat is expected to have slightly higher resistivity with respect to the underlying clayey
411 materials, with resistivity values for the peat in the order of 20-50 Ω·m (compare e.g.
412 with Kowalczyk et al., 2017). Ground-contact geophysical methods, such as ERT, have
413 been extensively used in previous studies to resolve peat thickness and electrical
414 characteristics (Boon et al., 2008; Comas et al., 2015; Elijah et al., 2012). Our

415 experience confirms that ERT, applied to our study site, provides excellent results and
416 high-resolution imaging, and is able to discern peat resistivity properties from the
417 silty/clayey layers. However, when the peat layer is thin, ERT data must be collected
418 with very small electrodes spacing in order to characterize the peat with high vertical
419 resolution. In our case study, for example, we used a distance between electrodes of 0.5
420 m, and a better resolution would require an even smaller spacing. This implies that if
421 the targets are thin peat layers, and the area to be covered is large, field_–work can
422 quickly become overwhelming in terms of time and manpower. Thus, a demand for
423 faster and still accurate subsoil investigation methods is pressing.
424 Contact-less methods, if properly applied, have the advantage of providing fast results
425 for the characterization of large territories. Moreover, contact-less instruments can be
426 easily carried for long distances, across difficult-to-access territories, permanently
427 flooded or covered with dense vegetation. Our results show that such methods can be
428 very effective in detecting the presence of peat layers, both from ground based and
429 helicopter deployed sensors (i.e. FDEM and AEM method respectively). We show that,
430 if compared to the results obtained with ERT at the Zennare site, the contact-less ground
431 based FDEM technique and the remote airborne EM are both able to detect the presence
432 of the peat layer patterns and estimate the same range of resistivity values for peat and
433 subsoil. Our results show that, for conductive substrates, the peat presence can be
434 detected using AEM even when the peat layer is very thin; however, we also show that
435 AEM tends to overestimate the peat thickness. This result confirms the tendency of
436 AEM to overestimating thin peat layers that was found by Silvestri et al. (2019b) in
437 case of peats over conductive substrates in an Indonesian study site. On the contrary,
438 FDEM shows a superior accuracy in resolving the peat thickness, even for very thin
439 peat deposits. If we consider 12 Ω·m as the threshold value that separates the peat layer

from the substrate, we have on average a difference of less than 10 cm between the average peat thickness resolved by the FDEM instrument along the transect and the average thickness measured through probing. Such difference increases to 130 cm for the AEM data. Even if we must notice that the AEM flight lines do not overlap with the FDEM/ERT transect, we speculate that the difference is mainly due to the low vertical resolution of the AEM and not to an actual variability of the peat layer thickness, which is highly unfeasible at this study site. Note that, had we performed a contemporary FDEM and AEM campaign over common transects, a joint inversion of ground-based and airborne EM data would be possible and may potentially improve the final accuracy of the retrievals.

These considerations open up to new perspectives for the characterization of extended peatlands with contact-less and, in general, remote geophysical methods.

## 6. Conclusions

Contact-less electromagnetic methods represent a valid alternative to classic ground-based geophysical methods for peat thickness detection. ~~Selected a~~A peatland located South of the Venice lagoon (Italy) was selected as our study site~~,~~; we compared the results obtained by the inversion of multi-frequency ground-based FDEM and airborne time domain EM data to data coming from direct probing and detailed high resolution ERT.

The inverted results obtained from FDEM and AEM are in agreement with those obtained with the ERT detecting a resistive peat layer lying over a conductive clay substrate: the upper layer, about 1 m thick, shows a slightly larger electrical resistivity (> 25 Ω·m) than the underlying conductive layer with lower resistivity (< 12 Ω·m).

**Commented [DSSP5]:** Lines 459-460: Delete the word "Selected" in line 459 and add "as our study site" in line 460.

These features are in agreement with the information available on the site from shallow borehole drilling, confirming a peat thickness that varies between 80 cm and 130 cm across the selected transect, over a silty/clayey substrate.

Our results show that both contact-less electro-magnetic methods used in this study (FDEM and AEM) are effective in detecting the presence and electrical characteristics of peat layers over conductive substrates, potentially allowing for very fast and extended exploration surveys over large peatland sites, with a large saving of time and fieldwork if compared to traditional ground-based methods. The main difference between the two contact-less methods tested in our work lies on the accuracy in resolving the peat thickness. If the peat deposit thickness is large, the airborne AEM method can be adopted, allowing high accuracies over large territories (Silvestri et al., 2019a, 2019b). In case of thin peat deposits, FDEM provides higher vertical resolutions than AEM, substantially increasing the peat thickness mapping accuracy. We speculate that ground-based and airborne data can be used in a joint inversion scheme, with the purpose of enhancing AEM resolution where ground-based EM data are available and extend the results to larger areas where only AEM might be available in an upscaling effort: this will be the goal of near to come future studies.

Based on our results we conclude that the use of contact-less electro-magnetometer surveys hold the promise of becoming basic tools for peat thickness mapping, ~~a~~ necessary information in order to characterize these valuable natural carbon reservoirs.

**Commented [DSSP6]:** Lines 485-486: As "information" is used as a plural noun here, I suggest deleting the indefinite article "a" at the end of line 485.

**Acknowledgements**

This research is part of the project CReScenDo (Combining Remote Sensing Technologies for Peatland Detection and Characterization) that has received funding

from the European Union's Horizon 2020 research and innovation programme under the Marie Skłodowska-Curie grant agreement No. 747809.

AEM data are from the Flagship Project RITMARE – The Italian Research for the Sea – coordinated by the Italian National Research Council and funded by the Italian Ministry of Education, University and Research within the National Research Program 2011–2013.

The authors declare the following competing interests: Andrea Viezzoli is the head of a small company that provides technical support for the analyses of AEM data.

FDEM and ERT data used for this paper are freely available through OpenAIRE/Zenodo ~~at http:// ...~~ with DOI: 10.5281/zenodo.3786404.

**References**

Ballhorn, U., Jubanski, J., Siegert, F., 2011. ICESat/GLAS Data as a Measurement Tool for Peatland Topography and Peat Swamp Forest Biomass in Kalimantan, Indonesia. Remote Sens., 3, 1957-1982.http://doi.org/10.3390/rs3091957.

Ballhorn, U., Siegert, F., Mason, M., Limin, S., 2009. Derivation of burn scar depths and estimation of carbon emissions with LIDAR in Indonesian peatlands. Proceedings of the National Academy of Sciences of the United States of America, 106(50), 21,213–21,218, https://doi.org/10.1073/pnas.0906457106.

Binley, A., 2015. Tools and Techniques: DC Electrical Methods, in: Schubert, G. (Ed.), Treatise on Geophysics, 2nd Edition, Elsevier, Vol. 11, 233-259. http://doi.org/10.1016B978-0-444-53802-4.00192-5.

Boaga, J., Ghinassi, M., D'Alpaos, A., Deidda, G.P., Rodriguez, G., Cassiani, G., 2018. Geophysical investigations unravel the vestiges of ancient meandering channels and

511 their dynamics in tidal landscapes. Scientific Reports, 8:1708.
512 http://doi.org/10.1038/s41598-018-20061-5.
513 Boaga, J., 2017. The use of FDEM in Hydrogeophysics, Journal of Applied
514 Geophysics. http://doi.org/10.1016/j.jappgeo.2017.02.011.
515 Boaga, J., D'Alpaos, A., Cassiani, G., Marani, M., Putti, M., 2014. Plant-soil
516 interactions in salt marsh environments: Experimental evidence from electrical
517 resistivity tomography in the Venice Lagoon. Geophys. Res. Lett., 41, 6160–6166.
518 http://doi.org/10.1002/2014GL060983.
519 Boon, D., Kessler, H., Raines, M., Kuras, O., Auton, C., Williams, J., et al., 2008.
520 Modelling Scottish peat stratigraphy using integrated electrical geophysics.
521 [Lecture] In: Reinforced water: Engineering and environmental considerations in
522 construction over peat, Edinburgh, Scotland, 11 March 2008.
523 http://nora.nerc.ac.uk/id/eprint/4830/
524 Bourgeau-Chavez, L.L., Endres, S.L., Graham, J.A., Hribljan, J.A., Chimner, R.A.,
525 Lillieskov, E.A., Battaglia, M.J., 2018. Mapping peatlands in boreal and tropical
526 ecoregions, in: Liang, S. (Ed.), Comprehensive Remote Sensing, vol. 6. Oxford,
527 UK: Elsevier: 24–44., pp. 24-44.
528 Carbognin, L., Tosi, L., 2003. Il Progetto ISES per l'analisi dei processi di intrusione
529 salina e subsidenza nei territori meridionali delle Province di Padova e Venezia,
530 Grafiche Erredici, Padova (Italy), 95 pp.
531 Cassiani, G., Bruno, V-, Villa, V., Fusi, N., Binley, A.M., 2006. A saline tracer test
532 monitored via time-lapse surface electrical resistivity tomography. Journal of
533 Applied Geophysics, 59, 244-259, http://doi.org/10.1016/j.jappgeo2005.10.007.
534 Città Metropolitana Venezia: http://webgis.cittametropolitana.ve.it/geologia,
535 http://difesasuolo.provincia.venezia.it/DifesaSuolo/Index?pagina=1&id=banca_da

ti_idrogeologica, Banca dati geologica e idrogeologica, last access: 30 December 2017.

Comas, X., Slater, L., 2004. Low-frequency electrical properties of peat. Water Resources Research, 40, W12414. https://doi.org/10.1029/2004WR003534.

Comas, X., Terry, N., Slater, L., Warren, M., Kolka, R., Kristiyono, A., Sudiana, N., Nurjaman, D., Darusman, T., 2015. Imaging tropical peatlands in Indonesia using ground-penetrating radar (GPR) and electrical resistivity imaging (ERI): Implications for carbon stock estimates and peat soil characterization. Biogeosciences, 12(10), 2995–3007. https://doi.org/10.5194/bg - 12 - 2995 - 2015.

Comas, X.; Terry, N.; Hribljan, J.; Lilleskov, E. A.; Suarez, E.; Chimner, R. A.; and Kolka, R. K. 2017. Estimating belowground carbon stocks in peatlands of the Ecuadorian páramo using ground penetrating radar (GPR). *Journal of Geophysical Research-Biogeosciences* , 122, doi:10.1002/2016JG003550.

Da Lio, C., Tosi, L., Zambon, G., Vianello, A., Baldin, G., Lorenzetti, G., Manfe, G., Teatini, P., 2013. Long-term groundwater dynamics in the coastal confined aquifers of Venice (Italy). Estuar. Coast. Shelf Sci., 135, 248-259. https://doi.org/10.1016/j.ecss.2013.10.021.

de Franco, R., Biella, G., Tosi, L., Teatini, P., Lozej, A., Chiozzotto, B., Giada, M., Rizzetto, F., Claude, C., Mayer, A., Bassan, V. and Gasparetto-Stori, G., 2009. Monitoring the saltwater intrusion by time lapse electrical resistivity tomography: The Chioggia test site (Venice Lagoon, Italy). J. Appl. Geophys., 69, 117-130. https://doi.org/10.1016/j.jappgeo.2009.08.004.

Field Code Changed

Formatted: English (United States)

Formatted: English (United States)

559 Deidda, G.P., Díaz de Alba, P., Fenu, C, Lovicu, G., Rodriguez, G., 2019. FDEMtools:
560 a MATLAB package for FDEM data inversion. Numerical Algorithms.
561 https://doi.org/10.1007/s11075-019-00843-2 (in press).
562 Deidda, G.P., Díaz de Alba, P., Rodriguez, G., 2017. Identifying the magnetic
563 permeability in multi-frequency EM data inversion. Electron. Trans. Numer. Anal.,
564 47,1–17. http://doi.org/10.1553/etna_vol47s1.
565 Deidda, G.P., Díaz de Alba, P., Rodriguez, G., Vignoli, G., 2020. Inversion of
566 Multiconfiguration Complex EMI Data with Minimum Gradient Support
567 Regularization: A Case Study. Mathematical Geosciences.
568 https://doi.org/10.1007/s11004-020-09855-4 (in press).
569 Deidda, G.P., Fenu, C., Rodriguez, G., 2014. Regularized solution of a nonlinear
570 problem in electromagnetic sounding. Inverse Probl., 30 (12).
571 http://dx.doi.org/10.1088/0266- 5611/30/12/125014.
572 Draper, F.C., et al., 2014. The distribution and amount of carbon in the largest peatland
573 complex in Amazonia. Environ. Res. Lett., 9. http://doi.org/10.1088/1748-
574 9326/9/12/124017.
575 Elijah, A.A., Folorunso, A., Olubunmi, J., 2012. An application of 2D electrical
576 resistivity tomography in geotechnical investigations of foundation defects: A case
577 study. Journal of Geology and Mining Research, 3(12), 142–151.
578 http://doi.org/10.5897/JGMR12.002.
579 FAOSTAT 2013. FAOSTAT database. Food and Agriculture Organization of the
580 United Nations. Available at: http: / / faostat.fao.org /
581 Fenner, N., Freeman, C., 2011. Drought-induced carbon loss in peatlands. Nature
582 Geoscience 4, 895–900.http://doi.org/10.1038/ngeo1323.

Field Code Changed
Formatted: English (United States)
Formatted: English (United States)

583 Gambolati, G., Putti, M., Teatini, P., Camporese, M., Ferraris, S., Gasparetto Stori, G.,
584 Nicoletti, V., Silvestri, S., Rizzetto, F., Tosi, L., 2005. Peat land oxidation enhances
585 subsidence in the venice watershed. EOS, TRANSACTIONS, vol. 86, p. 217-
586 220,http://doi.org/10.1029/2005EO230001.
587 Gasparetto-Stori, G., Strozzi, T., Teatini, P., Tosi, L., Vianello, A., Wegmüller, U.,
588 2012. Dem of the Veneto plain by ERS2-ENVISAT cross interferometry, in:
589 Scappini, S., Zapparoli, S. (Eds.), 7th EUREGEO, European Congress on Regional
590 Geoscientific Cartography and Information Systems, vol. I, Centro Stampa Regione
591 Emilia-Romagna Publ (2012), pp. 345-350.
592 Gatti, P., Bonardi, M., Tosi, L., Rizzetto, F., Putti, M., Teatini, P., 2002. The peat
593 deposit of the subsiding Zennare Basin, South of Venice Lagoon, Italy:
594 geotechnical classification and preliminary mineralogical characterization, in:
595 Campostrini, P. (Ed.), Scientific research and safeguarding of Venice, CoRiLa
596 Research Program 2001 Results. p. 241-258, Venezia: Corila- Istituto Veneto
597 Scienze Lettere ed Arti, ISBN: 88-88143-12-2.
598 Holden, N.M., Connolly, J., 2011. Estimating the carbon stock of a blanket peat region
599 using a peat depth inference model. Catena, 86(2), 75–85.
600 Hooijer, A., Page, S., Jauhiainen, J., Lee, W.A., Lu, X.X., Idris, A., Anshari, G., 2012.
601 Subsidence and carbon loss in drained tropical peatlands. Biogeosciences, 9(3),
602 1053-1071. http://doi.org/ 10.5194/bg-9-1053-2012.
603 Householder, J.E., Janovec, J., Tobler, M., Page, S., Lähteenoja, O., 2012. Peatlands of
604 the Madre de Dios River of Peru: Distribution, geomorphology, and habitat
605 diversity, Wetlands, 32(2), 359–368.

606 Huang, H. Won, I.J., 2003. Real-time resistivity sounding using a hand-held broadband
607 electromagnetic sensor. Geophysics, 68, 1224–31.
608 https://doi.org/10.1190/1.1598114.
609 Jaenicke, J., Rieley, J.O., Mott, C., Kimman, P., Siegert, F., 2008. Determination of the
610 amount of carbon stored in Indonesian peatlands. Geoderma, 147, 151-158.
611 https://doi.org/10.1016/j.geoderma.2008.08.008.
612 Joosten, H., 2010. The Global Peatland CO2 Picture: Peatland Status and Drainage
613 Related Emissions in All Countries of the World. Wetlands International,
614 Wageningen, Netherlands, 36 pp.
615 Keaney, A., McKinley, J., Graham, C., Robinson, M., Ruffell, A., 2013. Spatial
616 statistics to estimate peat thickness using airborne radiometric data. Spatial
617 Statistics, 5, 3-24. https://doi.org/10.1016/j.spasta.2013.05.003.
618 Kowalczyk, S., Żukowska, K. A., Mendecki, M. J., Łukasiak, D., 2017. Application of
619 electrical resistivity imaging (ERI) for the assessment of peat properties: A case
620 study of the Całowanie Fen, Central Poland. Acta Geophysica, 65(1), 223–235.
621 https://doi.org/ 10.1007/s11600-017-0018-9.
622 McNeill, J.D., 1980. Electromagnetic terrain conductivity measurement at low
623 induction numbers. Tech. Rep. Technical Note TN-6. Geonics Limited.
624 Nicoletti, V., Silvestri, S., Rizzetto, F., Tosi, L., Putti, M., Teatini, P., 2003. Use of
625 remote sensing for the delineation of surface peat deposits south of the Venice
626 Lagoon (Italy). IGARSS 2003. International Geoscience and Remote Sensing
627 Symposium, vol. IV. Institute of Electrical and Electronics Engineers, Inc., pp.
628 2881–2883. CD-ROM.

Page, S.E., Siegert, F., Rieley, J.O., Boehm, H.V., Jaya, A., Limin, S., 2002. The amount of carbon released from peat and forest fires in Indonesia during 1997. Nature, 420(6911), 61–65. https://doi.org/10.1038/nature01131.

Parry, L.E., West, L.J., Holden, J., Chapman, P.J., 2014. Evaluating approaches for estimating peat depth. J. Geophys. Res. Biogeosci., 119, 567–576. http://doi.org/10.1002/2013JG002411.

Parsekian, A.D., Slater, L., Ntarlagiannis, D., Nolan, J., Sebesteyen, S.D., Kolka, R.K., Hanson, P.J., 2012. Uncertainty in peat volume and soil carbon estimated using ground-penetrating radar and probing. Soil Science Society of America Journal, 76(5), 1911-1918. http://doi.org/10.2136/sssaj2012.0040.

Rizzetto, F., Tosi, L., Carbognin, L., Bonardi, M., Teatini, P., 2003. Geomorphological setting and related hydrogeological implications of the coastal plain south of the Venice Lagoon (Italy), in Hydrology of the Mediterranean and Semiarid Regions, edited by E. Servat et al., IAHS Publ., 278, 463–470.

Silvestri, S., Christensen, C. W., Lysdahl, A.O.K., Anschütz, H., Pfaffhuber, A.A., Viezzoli, A., 2019a. Peatland volume mapping over resistive substrates with airborne electromagnetic technology. Geophysical Research Letters, 46(12), 6459-6468. https://doi.org/10.1029/2019GL083025

Silvestri, S., Knight, R., Viezzoli, A., Richardson, C. J., Anshari, G. Z., Dewar, N., Flanagan, N., Comas, X. 2019b. Quantification of Peat Thickness and Stored Carbon at the Landscape Scale in Tropical Peatlands: A Comparison of Airborne Geophysics and an Empirical Topographic Method, J. of Geophysical Research: Earth Surface, 124, pp. 1 – 17.

652 Slater, L. D., Reeve, A., 2002. Investigating peatland stratigraphy and hydrogeology
653 using integrated electrical geophysics. Geophysics, 67(2), 365–378.
654 https://doi.org/10.1190/1.1468597.
655 Sørensen, K. I., & Auken, E. (2004). SkyTEM – A new high ‐ resolution helicopter
656 transient electromagnetic system. Exploration Geophysics, 35(3), 191–199.
657 Teatini, P., Tosi, L., Viezzoli, A., Baradello, L., Zecchin, M., Silvestri, S., 2011.
658 Understanding the hydrogeology of the Venice Lagoon subsurface with airborne
659 electromagnetics. Journal of Hydrology, vol. 411, p. 342-354, ISSN: 0022-
660 1694.http://doi.org/ 10.1016/j.jhydrol.2011.10.017.
661 Teatini, P., Tosi, L., Viezzoli, A., Baradello, L., Zecchin, M. and Silvestri, S., 2011.
662 Understanding the hydrogeology of the Venice lagoon subsurface with airborne
663 electromagnetics. Journal of Hydrology, 411(3-4), 342-354.
664 https://doi.org/10.1016/j.jhydrol.2011.10.017.
665 Tosi, L., Carbognin, L., Teatini, P., Rosselli, R., Gasparetto Stori, G., 2000. The ISES
666 Project subsidence monitoring of the catchment basin south of the Venice Lagoon
667 (Italy). In: Carbognin, L., Gambolati, G., Johnson A.I., (Eds.). Land Subsidence,
668 vol. II, p. 113-126, Perugia: C.N.R., Gruppo nazionale per la difesa dalle catastrofi
669 idrogeologiche, ISBN: 88-87222-06-1.
670 Tosi, L., Teatini, P., Carbognin, L., Brancolini, G., 2009. Using high resolution data to
671 reveal depth-dependent mechanisms that drive land subsidence: the Venice coast,
672 Italy. Tectonophysics, 474, 271–284. https://doi.org/10.1016/j.tecto.2009.02.026.
673 Tosi, L., Teatini, P., Strozzi, T., Carbognin, L., Brancolini, G., Rizzetto, F., 2010.
674 Ground surface dynamics in the northern Adriatic coastland over the last two
675 decades. Rendiconti Lincei, 21 (Suppl. 1) (2010), pp. 115-129
676 https://doi.org/10.1007/s12210-010-0084-2.

677 Tosi, L., Da Lio, C., Strozzi, T., Teatini, P., 2016. Combining L- and X-Band SAR
678 Interferometry to Assess Ground Displacements in Heterogeneous Coastal
679 Environments: The Po River Delta and Venice Lagoon, Italy. Remote Sens, 8, 308.
680 https://doi.org/10.3390/rs8040308.
681 Tosi, L., Da Lio, C., Teatini, P., Menghini, A., and Viezzoli, A., 2018. Continental and
682 marine surficial water – groundwater interactions: the case of the southern coastland
683 of Venice (Italy), Proc. IAHS, 379, 387–392. https://doi.org/10.5194/piahs-379-
684 387-2018.
685 Turetsky, M.R., Benscoter, B., Page, S., Rein, G., van der Werf, G.R., Watts, A.e, 2015.
686 Global vulnerability of peatlands to fire and carbon loss. Nature Geoscience, 8, 11-
687 14 (2015). http://doi.org/10.1038/NGEO2325.
688 Van Asselen, S., Erkens, G., Stouthamer, E., Woodlerink, H. A. G., Geeraerts, R.E.E.,
689 Hefting, M.M., 2018. The relative contribution of peat compaction and oxidation to
690 subsidence in built-up areas in the Rhine-Meuse delta, The Netherlands. Science of
691 the Total Environment, 636, 177– 191.
692 https://doi.org/10.1016/j.scitotenv.2018.04.141.
693 Viezzoli, A., Christiansen, A.V., Auken, E., Sørensen, K.I., 2008. Quasi-3D modeling
694 of airborne TEM data by spatially constrained inversion. Geophysics, 73(3), F105–
695 F113. https://doi.org/10.1190/1.2895521.
696 Viezzoli, A., Tosi, L., Teatini, P., Silvestri, S., 2010. Surface water-groundwater
697 exchange in transitional coastal environments by airborne electromagnetics: the
698 Venice Lagoon example. Geophys. Res. Lett., 37, L01402, 2010.
699 https://doi.org/10.1029/2009GL041572.
700 Walter, J., Lück, E., Heller, C., Bauriegel, A. and Zeitz, J., 2019. Relationship between
701 electrical conductivity and water content of peat and gyttja: implications for

Field Code Changed

Field Code Changed

electrical surveys of drained peatlands. Near Surface Geophysics, 17(2), pp.169-179.

Zanello, F., Teatini, P., Putti, M., Gambolati, G., 2011. Long term peatland subsidence: Experimental study and modeling scenarios in the Venice coastland. Journal of Geophysical Research: Earth Surface, 116(F4). https://doi.org/10.1029/2011JF002010.

## Appendix

a

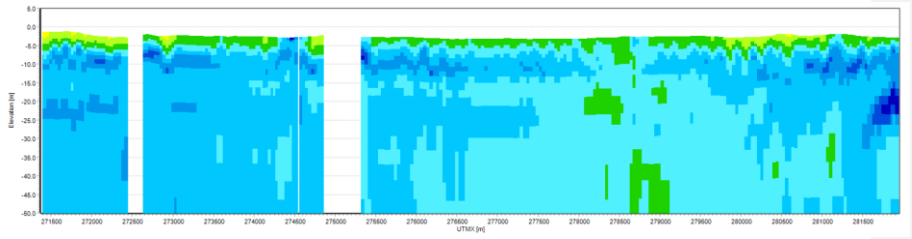

b

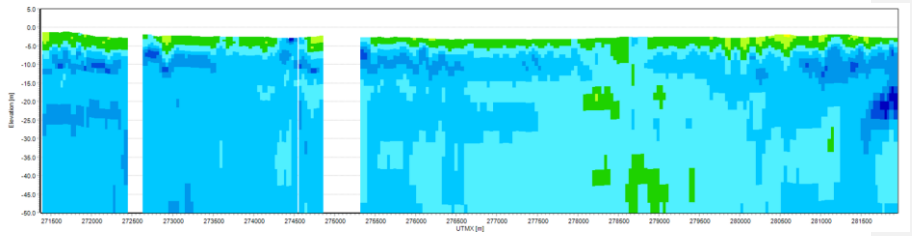

c

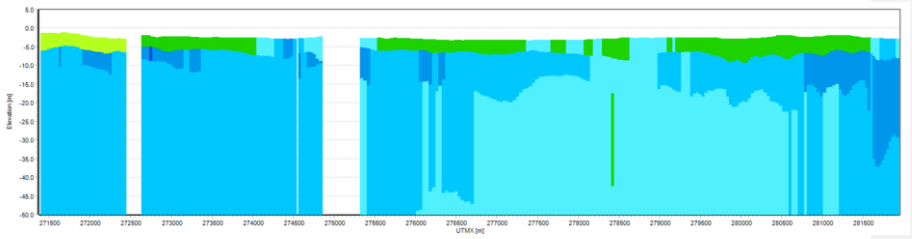

d

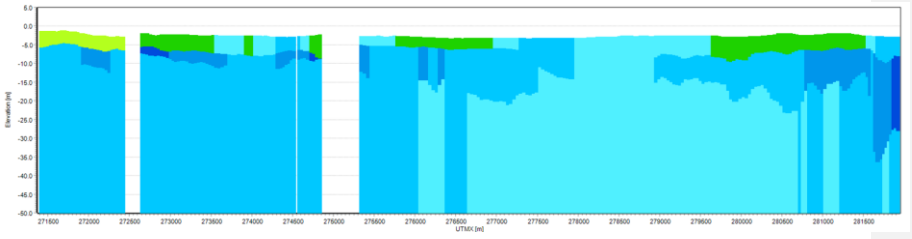

Fig. A1 – AEM resistivity model retrieved for the longest (northern) flight line using: a) 40 layers and starting with initial conductivity of 30 Ω·m; b) 40 layers and starting with initial conductivity of 5 Ω·m; c) 5 layers and starting with initial conductivity of 30 Ω·m; d) 5 layers and starting with initial conductivity of 5 Ω·m.